

The Quantum Yield of NO₃ from Peroxyacetyl Nitrate Photolysis

Troy L. Mazely[#], Randall R. Friedl^{*}, and Stanley P. Sander

Jet Propulsion Laboratory

California Institute of Technology

4800 Oak Grove Dr.

Pasadena, CA 91109

Peroxyacetyl nitrate (PAN) vapor was photolyzed at 248 nm and the NO₃ photoproduct was detected by laser induced fluorescence. The quantum yield for the production of NO₃ was determined by comparison to N₂O₅ photolysis data taken under identical experimental conditions. Contributions to the observed laser induced fluorescence were found to arise from excited state photoproducts such as NO₂^{*}. The excited state fluorescence contributions were investigated and a data analysis methodology was established to minimize their effects. The average of data collected over a range of total pressures, precursor concentrations, and buffer gases was 0.3 ± 0.1 for the NO₃ quantum yield, where the quoted statistical uncertainty represents two standard deviations. This result, combined with our previously reported value of 0.83 ± 0.09 for the NO₂ quantum yield from the photolysis of PAN, suggests that NO₂ and NO₃ represent the only nitrogen containing products in the 248 nm photolysis of PAN. The atmospheric implications of a NO₃ producing channel in PAN photolysis are considered.

[#]present address: Logicon Geodynamics, Inc., Torrance, CA, 90501

^{*} to whom correspondence should be addressed

Introduction

In addition to its well-known role in urban pollution, **peroxyacetyl** nitrate or PAN, $\text{CH}_3\text{C}(\text{O})\text{OONO}_2$, has received increasing attention for its importance as an intermediate in the redistribution of reactive odd-nitrogen, NO_x (i.e. $\text{NO} + \text{NO}_2$), from source regions to remote locations.² The capability of PAN, following its formation from the reaction of **peroxyacetyl** radicals with NO_2 ,³ to transport NO_x over long distances stems from the strong dependence of its lifetime on temperature.⁴⁻⁶ This is particularly true in the lower troposphere where changes in local meteorology can translate to order of magnitude changes in the thermal lifetime of PAN. At higher altitudes, where PAN has a long thermal lifetime, **photolysis** of PAN gains in importance as a pathway for release of NO_x , becoming the dominant pathway at altitudes greater than approximately 7 km.⁷ Consequently, the role of PAN in NO_x and O_3 chemistry of the upper troposphere is related to the rates and mechanisms of the **photolysis** process.

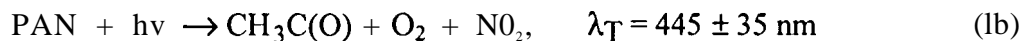
Recently, we quantified the yield of NO_2 from the 248 nm **photolysis** of PAN.⁸ In those experiments the production of NO_2 , from measured concentrations of PAN, was compared to NO_2 produced from **photolysis** of known amounts of HNO_3 . The same experimental conditions were maintained for each data set, A quantum yield of 0.83 ± 0.09 for NO_2 production was deduced from the experiments, where the quoted error represents two standard deviations in precision. This quantum yield result establishes NO_2 as the major nitrogen containing product from the 248 nm **photolysis** of PAN; however, it also supports the likelihood of small, but non-negligible, yields of other nitrogen containing products.

Combination of the NO_2 quantum yield result with information on internal energy disposal in the NO_2 **photofragment** indicates that the operative **photolytic** pathway for NO_2

production is through either a direct (ie. simple bond fission)



or concerted mechanism



where the listed threshold wavelengths are for 298 K. ⁹

In the atmosphere, both channels ultimately lead to regeneration of NO_2 and the peroxyacetyl radical ($\text{CH}_3\text{C}(\text{O})\text{O}_2$). Because atmospheric PAN is largely formed from the three body combination of NO_2 and $\text{CH}_3\text{C}(\text{O})\text{O}_2$, reaction pathways 1a and 1 b lead to chemical null cycles and restrict the role of PAN at higher altitudes to that of a temporary odd nitrogen and carbon reservoir and a transport vehicle of these species from source regions to remote locations.

Photolysis channels of PAN leading to odd nitrogen species other than NO_2 , *viz.* NO or NO_3 , are of interest since they represent sources of additional atmospheric odd oxygen. The lowest energy pathway involves NO_3 production by direct bond fission, *i.e.*



Subsequent photolysis of the NO_3 product in the atmosphere occurs rapidly and will yield atomic oxygen and NO_2 ; a net increase in odd oxygen. The unstable $\text{CH}_3\text{C}(\text{O})\text{O}$ product of channel 2 will decompose into CO_2 and CH_3 and the subsequent oxidation of the methyl radical will also net additional odd oxygen. ¹⁰

In this work we have investigated NO_3 production from the photolysis of PAN at 248 nm. The NO_3 was detected by laser induced fluorescence (LIF). By comparison to NO_3 production from photolysis of N_2O_5 under identical experimental conditions, we have determined a relative quantum yield for the production of NO_3 from PAN. The implications of these results to the atmosphere will be presented.

Experiment

Descriptions of our pulsed photolysis LIF detection instrument have been presented previously.^{8,11} Consequently, only details pertinent to understanding the present work will be discussed. Gaseous samples of N_2O_5 and PAN were introduced into the flowing system by passing a carrier gas (He, Ar, or O_2) through a pyrex reservoir containing gaseous PAN or N_2O_5 in equilibrium with solid samples of the compounds. The vapor concentrations of both N_2O_5 and the PAN were determined by optical absorption in a 50 cm long absorption cell upstream of the photolysis chamber. The 254 nm emission line of a low pressure Hg lamp and the 214 nm emission line from a Zn lamp were employed in the respective N_2O_5 and PAN absorption measurements. The pressures in the reservoir and absorption cell (25- 150 Torr) were controlled by a downstream needle valve and monitored with an MKS Baratron capacitance manometer. All flows rates were determined using calibrated flow meters.

The N_2O_5 was synthesized by reacting NO_2 , which was purified by several freeze/thaw cycles in an oxygen rich environment, with O_3 . The synthesis involved mixing a flow of gaseous NO_2 , obtained by directing the vapor from a 25 °C liquid NO_2 sample, into a pyrex tubular reactor with a flow of O_3 in O_2 that was generated by a commercial ozonizer. The mixture was allowed to react for approximately 20 ms (i.e. flow time to trap) to insure complete reaction. The N_2O_5 formed in this process was collected in a reservoir which was cooled by a 2-propanol/dry ice slush (-78° C). The synthesized N_2O_5 was subsequently stored at -196° C in a liquid nitrogen bath. During photolysis experiments, the N_2O_5 sample was maintained at a constant temperature of approximately -15°C.

The PAN samples were prepared by the method of Gaffney *et al.*² Briefly, the synthesized PAN vapor was extracted from an organic solvent and collected in a vessel held at -196° C. Batches of frozen PAN were stored in the dark at this temperature.

During **photolysis** experiments the PAN samples were maintained at a temperature of either -48°C using a *n*-hexanol slush or approximately -20°C using an aqueous CaCl_2 slush. The PAN was found to be quite stable with respect to decomposition at these temperatures; however, safety precautions against explosions, in the form of plexiglass shielding, were employed when handling the substance because previous investigators have documented explosive decomposition of PAN under some conditions.

The concentrations of N_2O_5 and PAN in the **photolysis** cell ranged between $(0.5 \text{ and } 5.0) \times 10^4 \text{ cm}^{-3}$ (i.e. 1.5- 15 mTorr) while the total pressures in the **photolysis** cell ranged from 100 mTorr to 20 Torr. Quantum yield determinations were only made for measurements with total pressures greater than 2 Torr. At those partial pressures NO_3 fluorescence quenching was primarily due to the carrier gas rather than the NO_3 precursors. In order to **simplify** quantum yield determinations the optical densities of PAN and N_2O_5 in the **photolysis** cell were maintained, for any set of experiments, within approximately an order of magnitude of each other.

The weakly focused output of an excimer laser (Questek Model 2240) operating at 248 nm was used to **photolyze** the PAN and N_2O_5 . The repetition rate of the **excimer** (5-50 Hz) and the total gas flow rate through the **photolysis** cell (500-5000 seem) were adjusted to ensure that all **photoproducts** were removed from the detector viewing zone between laser shots. The energy density ranged from 35 to 75 mJ/cm^2 per pulse and the **photolytic** signal was observed to be linear with laser pulse energy.

Two laser systems were utilized for LIF detection of NO_3 . The first was comprised of a dye laser (Lambda Physik FL3001 with modified optics) pumped by a pulsed copper vapor laser (CVL: Oxford model CU 15A) operating at a selectable repetition rate between 4 and 20 kHz. The laser dye solution consisted of 0.15 g of **sulf-Rhodamine 640** and 0.40 g of Kiton Red per liter of ethanol. The employment of two dyes in the solution increased the efficiency of the dye laser because the absorption maxima of the respective dyes closely match the 511 and 578 nm output wavelengths of the CVL. We found that both the

lifetime and performance of the dye was greatly improved by cooling the solution with a closed loop liquid heat exchanger. A laser tuning range of 615 nm to 670 nm was achieved with this system.

The second laser system was comprised of a dye laser (Spectra Physics PDL-3) pumped with the 2W, 10HZ, 532 nm harmonic of a Nd:Yag (Spectra Physics GCR- 130-10). The dye employed in this system was DCM at concentrations of 26.8 mg/L and 180 mg/L (in ethanol) for use in the oscillator and **pre-amplifier** sections of the dye laser, respectively. The tuning range for the laser was between 605 nm to 670 nm. The majority of experimental data was obtained with this second laser system due its output power advantage; a result of the better dye laser conversion efficiency ($\cong 20\%$) as compared to the CVL system ($\cong 5-10\%$) which had a peak pulse energy that was near the **lasing** threshold of the dye.

The LIF signal was detected by a cooled photomultiplier tube (PMT:Burle C3 1034-02) that was oriented perpendicular to the laser beam axes. The LIF signal was amplified, discriminated, and counted on a multi-channel scaler card (MCS: Canberra Accuspec). A 650 nm long pass and a 750 nm short pass filter were placed in front of the PMT to block laser scatter and prevent detection of stray room light in the far red optical region, respectively. The photon collection geometry was significantly enlarged relative to our previous NO_2 yield studies. One consequence of this was that the rate of loss of NO_3 ($\approx 500 \text{ S}^{-1}$ in 1 torr He) from the viewing zone due to diffusion and bulk gas flow was less than in the previous studies.

The absorption spectrum of NO_3 is characterized by two major peaks; one near 623 nm and the other at 662 nm.⁹ Both of these wavelengths were investigated as potential excitation wavelengths of NO_3 . Preliminary investigations were performed by illuminating chemically produced NO_3 with the probe laser. For those tests, NO_3 was synthesized by reacting neat HNO_3 vapor with fluorine atoms which were formed by passage of molecular fluorine through a microwave discharge. The ratio of the NO_3 LIF signals at these two

wavelengths was found to correlate well with the ratio of the corresponding absorption cross sections of NO_3 . Even though the absorption cross section of NO_3 is nearly 50% larger at 662 nm than at 623 nm and approximately 15% of the NO_3 is photolyzed at 623 nm,³ we achieved much greater sensitivity (i.e. signal to noise) at 623 nm for two principal reasons. First, for both the Nd:YAG and CVL pump lasers, the dye laser had a greater lasing efficiency at 623 nm than at 662 nm. This was particularly true for the CVL pumped dye laser, since the dye laser was operating barely over the lasing threshold at 662 nm. Significant lowering of the 662 nm lasing threshold could not be achieved using a variety of other dye solutions.

Another advantage of 623 nm excitation relative to 662 nm excitation was that the latter wave length was within our detection band, while the former was not. On account of this, the excitation at 662 nm resulted in a large amount of laser scatter, thereby decreasing the signal to noise ratio relative to the 623 nm probe. We also tried other detection bandwidths, such as 700 nm to 750 nm, in order to block the 662 nm light; in all cases the 623 nm laser line proved to be more sensitive.

Although not critical to the quantum yield determination, we endeavored to calibrate the laser detection system. From these trials, a detection sensitivity of approximately $5 \times 10^8 \text{ NO}_3 \text{ cm}^{-3}$ was obtained for one minute of integration time of Nd:YAG pumped dye laser pulses (i.e. 600 shots). Since NO_3 concentrations were not measured independently, our LIF sensitivity estimate was based on a chemical kinetics simulation of the NO_3 concentration profiles resulting from the $\text{HNO}_3 + \text{F}$ reaction system. The CVL pumped probe gave integrated sensitivities that were similar to those obtained with the Nd-YAG pumped probe, however, the per pulse sensitivity of the CVL pumped probe was approximately three orders of magnitude less than the Nd:YAG pumped probe due to the large difference in laser repetition rates,

Results

Initial Experimental Observations. Temporal profiles of the signal were obtained for both the photolysis of PAN and N_2O_5 at total pressures ranging from 100 mTorr to 20 Torr. Background signals, originating from cell and filter fluorescence induced by the excimer laser, were readily removed from the data, leaving the residual probe laser signal for further analysis (see figure 1).

Based on our previous experience with NO_2 fluorescence detection we anticipated that bulk diffusion would control the temporal loss of NO_3 fluorescence signal above some minimum total pressure.^{8,11} Accordingly, we first attempted to represent the observed fluorescence decays with a single exponential expression,

$$S = S_0 e^{-k_{\text{loss}} t} + S_{\text{scatter}}, \quad (3)$$

where S_{scatter} represents the signal from probe laser scatter off chamber walls and k_{loss} represents the first order loss rate due to diffusion. When we set the value of k_{loss} to be of similar magnitude to the diffusion loss rates obtained in previous studies on the same apparatus, we found that equation 3 fit the data well only at long time scales ($t > 1$ ms) (see solid curve in figure 1). Relatively good fits could be obtained at short time scales, at the expense of the long time fit, if k_{loss} was increased substantially. However, the values of k_{loss} , derived from such fits did not depend, in a simple way, on total pressure as would be expected for diffusional loss (see figure 2). Furthermore, the observed loss rates obtained in this fashion, especially at the higher pressures, *i.e.* > 1 Torr, were much too large to be explained by pure bulk diffusion in our system. Consequently, we can not ascribe the observed temporal behavior of the fluorescence signal simply to NO_3 diffusion out of the detection zone.

The temporal evolution of the data was better described with the following biexponential fit (dashed curve in figure 1),

$$S = S_{\text{slow}} e^{-k_{\text{slow}} t} + S_{\text{fast}} e^{-k_{\text{fast}} t} + S_{\text{scatter}}, \quad (4)$$

where the first term on the right hand side of the equation dominates at long times and the second term dominates at short times. Derived values of k_{slow} were similar in magnitude to those expected for loss due to molecular diffusion ($k_{\text{slow}} \approx 500 \text{ s}^{-1}$ in 1 Torr He) and displayed the appropriate linear dependence on total pressure. The larger loss rates associated with k_{fast} were of the same magnitude as those measured previously for relaxation of vibrationally excited NO_2 from HNO_3 and PAN photolysis under similar pressure conditions ($k_{\text{fast}} \approx 5000\text{-}15000 \text{ s}^{-1}$ in 1 Torr He). To the extent that excited NO_2 can fluoresce in the bandwidth of our detection system, it represents an excellent candidate for explaining the data shown in figure 2. Alternatively, excited NO_3 might also be responsible for the rapidly decaying fluorescence. In either case, the observed quenching rates depend critically on the nascent population distribution and the functional dependence of quenching rates on internal excitation. Because of these dependence it is not possible to ascribe concrete physical interpretations to k_{slow} and k_{fast} . However, it is clear that k_{slow} has substantial diffusional character and k_{fast} is closely related to the quenching rates of excited states.

The possible impact of excited molecular photofragments on the observed fluorescence prompted us to characterize the signal as a function of excitation wavelength. The idea here was to establish the existence of excited photoproducts by observing fluorescence at off-resonance excitation wavelengths with respect to NO_3 . As a reference we also analyzed the excitation spectrum of a thermalized NO_3 distribution, produced from the reaction of F with HNO_3 (as described in the experimental section). As shown in figure 3, the observed LIF excitation spectrum of the thermalized NO_3 , normalized to a constant laser power over the wavelength range, correlates with the known NO_3 absorption spectrum. However, when NO_3 was generated photolytically from N_2O_5 , a variety of fluorescence excitation curves could be obtained, depending on the carrier gas identity, delay time between pump and probe laser, and total pressure. Figure 4 highlights some of the observations taken at a fixed, and relatively short delay time between the pump and

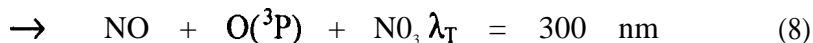
probe lasers, but at variable total pressures, At the higher pressure (7 torr), the observed fluorescence excitation spectra largely resembles the absorption spectrum of NO_3 , as was the case for the chemically formed NO_3 . However, at the lower pressure (1 torr) there is only a slight correlation between the LIF excitation and NO_3 absorption spectra, indicating that a substantial part of the LIF signal obtained under these conditions is due to species other than ground state NO_3 . The relative invariance of the LIF signal at 1 torr, with respect to excitation wavelength, requires that the additional fluorescing species possess continuum absorption spectra with cross sections on the same order as that of NO_3 at 623 nm. The continuum character of the fluorescence is quite consistent with the spectral characteristics of NO_2 .

Analysis of the temporal behaviors of fluorescence induced at various excitation wavelengths provided additional information on the identity of the fluorescing species. Figure 5 shows temporal profiles of fluorescence signal resulting from excitation at 623 nm and 635 nm; the latter wavelength corresponding to a local minimum in the absorption cross section of NO_3 (i.e. $\sigma(623 \text{ nm})/\sigma(635 \text{ nm}) = 11$). The data reveal two important pieces of information. First, at short times the absolute magnitude of the nascent LIF signal does not vary significantly between 623 nm and 635 nm, as would be expected based on the NO_3 cross-sectional difference. Second, retrieved values of the signal decay rate, k_{fast} (using eq. 4), were strikingly different for the two wavelengths; i.e. 5000 s^{-1} at 623 nm and 40000 s^{-1} at 635 nm. At a minimum, we interpret the large variation in k_{fast} to indicate that the fluorescence detected at 635 nm is predominated by species other than ground state NO_3 . Additionally, the absolute value of k_{fast} at 635 nm compares well with previous, independent determinations of the quenching rate for vibrationally excited NO_2 under similar pressure conditions, ” providing further evidence for the involvement of excited NO_2 in the present experiments. Assuming that the additional fluorescing species emit over a broad continuum, as would be the case for NO_2^* , then the 623 nm signal

obtained at short delay times (i.e. < 100 μs) is likely composed of significant contributions from both NO_2^* and NO_3 .

In summary, our initial observations of PAN and N_2O_5 photolysis provided strong evidence for LIF contributions in our detection bandpass (i.e. 650 nm and 750 nm) from species other than ground state NO_3 . The excitation wavelength dependence of the fluorescence intensities and lifetimes suggests that the primary additional fluorescing species is electronically/vibrationally excited NO_2 . Further evidence in support of this identification and strategies to derive NO_3 yields from the fluorescence signal are discussed in the next section.

Fluorescence Interference by NO_2 . The choice of N_2O_5 as a photolytic NO_3 reference derives from the results of previous N_2O_5 quantum yield determinations which indicate that NO_3 is the major nitrogen-containing photoproduct. Although N_2O_5 photolysis at 248 nm has four accessible channels



the majority of studies indicate that channels 5 and 8 predominate. Direct detection of NO_3 by optical absorption was utilized by Ravishankara *et al.* ¹⁴ and Swanson *et al.* ¹⁵ to derive NO_3 quantum yields of 1 and 0.89, respectively. Because of their relatively small absorption cross sections at 623 nm, the coincident production of ground state NO_2 and NO in N_2O_5 (PAN) photolysis do not pose a complication to LIF studies of NO_3 .

However, results from several studies have raised the possibility of significant production of excited state products. In particular, Ravishankara *et al.* ¹⁴ have speculated that atomic oxygen formation in N_2O_5 photolysis may be the result of unimolecular decomposition of internally excited NO_2 or NO_3 . In the Swanson *et al.* ¹⁵ study a growth in the NO_3 signal

was observed at early times following the **photolysis**; the origin of which was interpreted as being due to relaxation of excited nascent NO_3 . More recently, Oh *et al.*¹⁶ have analyzed the optical emission following laser photolysis of N_2O_5 and deduced that the **photolysis** products are NO_3 and a wavelength dependent mixture of NO_2 , NO_2^* , and $\text{NO} + \text{O}$, where NO_2^* is internally excited NO_2 . This inference about the presence of excited NO_2 is the same one that we have made in previous studies of HNO_3 and PAN **photolysis**, namely, that the majority of NO_2 formed during **photolysis** is electronically excited.

Based on our current data and on the previous data of Swanson *et al.*¹⁵ and Oh *et al.*¹⁶ we believe that some (@ 623 nm) or nearly all (@ 635 nm) of the LIF signal observed from N_2O_5 **photolysis**, under conditions where the photoproducts have experienced few collisions, is due to absorption by, and subsequent fluorescence of internally excited NO_2 . As discussed in the previous section, this hypothesis is supported qualitatively by the fluorescence decay rates observed for 635 nm excitation and by the continuum character of the fluorescence excitation spectrum. One apparent problem with this hypothesis is that NO_3 absorption cross sections in the 623 nm region are approximately 3 orders of magnitude larger than those of NO_2 . However, Corcoran *et al.*¹⁷ have shown that NO_2 cross sections rise significantly upon thermal heating of NO_2 . In particular, Corcoran *et al.*¹⁷ found that NO_2 absorption cross sections in the 610 nm region increase by an approximate factor of three between 300 K and 673 K. In the present case, the nascent population distribution of NO_2^* following N_2O_5 (and PAN) **photolysis** corresponds to a “thermal” distribution on the order of 10000 K. Extrapolation of the trend found by Corcoran *et al.*¹⁷ to internal temperatures encountered in the **photolysis** case yields NO_2 cross section values that are comparable to those of NO_3 .

From our initial observations we did not find clear evidence for the presence or absence of excited state NO_3 following **photolysis** of N_2O_5 or PAN. The impact of NO_3 , if present, on our quantum yield experiments would be quite different than NO_2^* , when one considers the energetic of the pump and probe steps. On the one hand, the probe laser

energy ($\cong 16,000 \text{ cm}^{-1}$) is only slightly less than the dissociation energy of ground state NO_3 ($\cong 17,300 \text{ cm}^{-1}$),¹⁸ insuring that even modestly excited NO_3 will photodissociate rather than fluoresce. Consequently, a LIF contribution from NO_3^* would be seen only after near complete quenching of NO_3 to low vibrational levels of the $^2\text{A}_2$ ground state. The time required to quench the remaining few vibrational quanta should be sufficiently short, at total pressures in the torr range, to render, as inconsequential, any difference between the LIF sensitivity of vibrationally excited and ground state NO_3 . Accordingly, any NO_3^* produced in the present experiments would appear as a time delayed population of ground state NO_3 and would be folded into the determination of the quantum yield for channel 2.

On the other hand, the LIF contribution of NO_2^* is confined to a narrow temporal window, commencing a few microseconds after the pump pulse and ending in tens of microseconds later. This behavior is related to the following spectral and experimental features: (a) For 248 nm photolysis the generated NO_2 molecules are created generally with more than 9100 cm^{-1} of internal energy, i.e. electronically excited, and initially are photodissociated by the probe laser rather than fluoresce. However, the electronic energy of the NO_2^* is interconverted to vibrational levels in the electronic ground state near 9100 cm^{-1} in less than $5 \mu\text{s}$; (b) The LIF sensitivity of NO_2^* below 9100 cm^{-1} is a strong, increasing, function of internal energy and is comparable to that of NO_3 only for internal energies above approximately 5000 cm^{-1} ; (c) The lifetime of NO_2^* at levels above 5000 cm^{-1} has been found in earlier studies¹¹ to be approximately $30 \mu\text{s}$ for the experimental pressure conditions used in the present experiment.

The above-given considerations suggest an experimental strategy that confines fluorescence detection to specific temporal windows ($> 100 \mu\text{s}$ after pump pulse) and experimental pressures ($> 2 \text{ torr}$). This strategy will maximize the quenching of excited NO_2 and NO_3 , thereby minimizing the LIF contribution from NO_2^* and maximizing the contribution from ground state NO_3 . Moreover, the continued collection of LIF data at 635 nm during quantum yield determinations presents itself as a means to correct for small

persisting contributions from NO_2^* . The correction methodology relies on the assumption that the NO_2^* contribution to the total signal at 623 nm is identical to the total signal observed at 635 nm. Under this assumption the NO_2^* contribution is removed simply by subtracting the two data sets. Upon first application of this procedure to the data, we noted that the residual signal displayed a growth rate at early times. Interpreting this growth as relaxation of excited NO_3 , we calculated relaxation rate coefficients that are in semi-quantitative agreement with the reported values of Swanson *et al.*⁶

Based upon our analysis of the preliminary data, we are convinced that all of our LIF data can be readily understood in terms of relaxation of excited NO_2 and NO_3 and the relative LIF sensitivities of ground and excited state NO_2 and NO_3 . Consequently, we believe that an experimental strategy employing appropriate total pressures, pump - probe synchronizations, and off-resonance background scans will yield a robust measure of the NO_3 quantum yield from PAN photolysis.

NO_3 Quantum Yields. A well known procedure for determining quantum yields is through use of a reference gas whose optical cross section and quantum yield are known.⁸ In the present experiments N_2O_5 was employed as the reference gas for determinations of the NO_3 quantum yield from PAN. By measuring relative NO_3 production from these two species, under otherwise identical experimental conditions, the NO_3 quantum yield for PAN could be obtained without a direct need for knowledge of the absolute detection sensitivity. The relative signal of NO_3 from each of the experiments is related to the quantum yield by

$$\frac{[\text{NO}_3]_{\text{PAN}}}{[\text{NO}_3]_{\text{N}_2\text{O}_5}} = \frac{\phi_{\text{PAN}}^{\text{NO}_3}(\lambda)}{\phi_{\text{N}_2\text{O}_5}^{\text{NO}_3}(\lambda)} \frac{[\text{PAN}]}{[\text{N}_2\text{O}_5]} \frac{\sigma_{\text{PAN}}}{\sigma_{\text{N}_2\text{O}_5}(\lambda)} \quad (9)$$

Rearrangement of this relation gives

$$\phi_{\text{PAN}}^{\text{NO}_3}(\lambda) = \phi_{\text{N}_2\text{O}_5}^{\text{NO}_3}(\lambda_{\text{photo}}) \frac{[\text{NO}_3]_{\text{PAN}}}{[\text{NO}_3]_{\text{N}_2\text{O}_5}} \frac{[\text{N}_2\text{O}_5]}{[\text{PAN}]} \frac{\sigma_{\text{N}_2\text{O}_5}(\lambda)}{\sigma_{\text{PAN}}(\lambda)} \quad (10)$$

In the present studies relative NO₃ concentrations were determined from measurements of LIF signal and initial precursor concentrations were obtained by measuring the optical absorbance at a particular absorption wavelength, A(λ_{abs}). Incorporating this into eq 10 results in

$$\phi_{\text{PAN}}^{\text{NO}_3}(\lambda_{\text{photo}}) = \phi_{\text{N}_2\text{O}_5}^{\text{NO}_3}(\lambda_{\text{photo}}) \frac{\text{LIF}_{\text{PAN}}(\tau) A_{\text{N}_2\text{O}_5}(\lambda_{\text{abs}}) \sigma_{\text{PAN}}(\lambda_{\text{abs}}) \sigma_{\text{N}_2\text{O}_5}(\lambda_{\text{photo}})}{\text{LIF}_{\text{N}_2\text{O}_5}(\tau) A_{\text{PAN}}(\lambda_{\text{abs}}) \sigma_{\text{N}_2\text{O}_5}(\lambda_{\text{abs}}) \sigma_{\text{PAN}}(\lambda_{\text{photo}})} \quad (11)$$

where Beer's Law

$$A_i = \sigma_i(\lambda_{\text{abs}}) L \quad [i] \quad (12)$$

was incorporated into the expression. In eq 11, LIE(T) is the LIF signal at a probe delay time τ . Because the same absorption cell was employed for measurements of the absorbance of each photolytic precursor, the cell path length, L, cancels out of the expression; however, different absorption wavelengths were used which are distinguished by an asterisk. Accurate application of eq 11 requires knowledge of the optical cross sections of each precursor at both the photolysis and absorption wavelengths.

The experimental measurements of the optical cross sections of PAN have been discussed in previous papers. For the analysis of the present data only the relative cross section at the photolysis and absorption wavelengths needs to be known. Averaging the results of Senum *et al.*¹⁹, Talukdar *et al.*⁷, and Libuda and Zabel²⁰ we derive a value of 10.0 ± 0.4 for the ratio of PAN absorption cross sections at 214 nm and 248 nm, i.e.

$$\frac{\sigma_{\text{PAN}}(\lambda_{\text{abs}} = 214\text{nm})}{\sigma_{\text{PAN}}(\lambda_{\text{photo}} = 248\text{nm})} = 10.0 \pm 0.4, \quad (13)$$

where the quoted uncertainty represents two standard deviations. Similarly the absorption cross sections for N₂O₅ were obtained from a data compilation and yielded a value of 1.32 for the ratio of cross sections at 248 nm and 254 nm, i.e.

$$\frac{\sigma_{\text{N}_2\text{O}_5}(\lambda_{\text{photo}} = 248\text{nm})}{\sigma_{\text{N}_2\text{O}_5}(\lambda_{\text{abs}} = 254\text{nm})} = 1.32. \quad (14)$$

The uncertainties in the cross sections of N_2O_5 at these wavelengths were not cited in the data compilation; however, the absorption spectrum for N_2O_5 is much better established than for PAN, causing the latter to dominate the uncertainty attached to our NO_3 quantum yield determination. The inclusion of the above-mentioned cross sectional ratios in equation 11 yields

$$\phi_{PAN}^{NO_3}(\lambda_{photo}) = (13.2 \pm 5.3) \times \frac{LIF_{PAN}(\tau) A_{N_2O_5}(\lambda_{abs} = 254nm)}{LIF_{N_2O_5}(\tau) A_{PAN}(\lambda_{abs} = 214nm)} \quad (15)$$

where the quoted uncertainty arises largely from uncertainties in the PAN cross sections. We have also used a value of unity for the NO_3 quantum yield from N_2O_5 photolysis. Based on previous literature we associate an uncertainty of 0.3 with the unity quantum yield determination. Note that eq 15 is now entirely composed of observable; the two absorbance and the relative fluorescence signal.

Photolysis data were collected at total pressures from 2 to 10 Torr in three different carrier gases; He, Ar, and O_2 . For the data acquired with the CVL probe the high repetition frequency resulted in acquisition of a LIF data point every 50 to 150 μs , depending on the repetition rate of the laser. An example of PAN data from the CVL probe is shown in figure 6. These data were further analyzed by ratioing absolute signals from each precursor at a fixed time delay, The average of all of these ratios determined the quantum yield of NO_3 from PAN. As stated in the previous section, for the low pressure data sets the early time data was not utilized in determining a quantum yield because a significant fraction of the photoproducts were excited and the fluorescent signal did not reflect the actual yield of ground state NO_3 .

For the data acquired with the Nd:Yag pumped probe the time delay between the pump and probe laser was fixed and sequential photolysis experiments were performed for each set of PAN and N_2O_5 concentrations. The time delay was chosen large enough such that complete relaxation of the internally excited photoproducts had occurred and short enough such that a significant fraction of the NO_3 remained in the viewing zone. Typically

the time delay was 100 μs at 10 Torr with progressively longer times at lower pressures. For a given experimental pressure condition the time delay was varied between approximately 30 μs and 2 ms in order to validate the independence of the results on the specific time delay.

The summary of data obtained over a range of total pressures, carrier gases, and concentrations of PAN is shown in Table 1. The production of NO_3 from PAN was observed consistently in all data sets. The values of the quantum yield at each of the pressure and carrier gas combination ranged from 0.2 to 0.4 with no dependence observed on either of these variables. The overall weighed average of the data set is 0.3 ± 0.1 , where the error represents two standard deviations in precision. In our previous investigation of PAN, a quantum yield for the production of NO_2 was measured to be 0.83 ± 0.09 . Combining the earlier result with the present result indicates that the photodissociation quantum yield at 248 nm is essentially unity with the only nitrogen-containing products being NO_2 and NO_3 . A variance weighted normalization of the two results yields quantum yields of 0.77 ± 0.08 and 0.23 ± 0.08 for NO_2 and NO_3 from PAN, respectively.

Summary and Discussion

Prior to an experimental determination of the NO_2 quantum yield from PAN photolysis, photochemical data compilations had considered channel 1 a, forming NO_2 and CH_3CO , to be the most likely PAN photochemical process. As a consequence, most tropospheric model calculations to date have assumed a unity quantum yield for 1a. Our recent investigation of the NO_2 yield from PAN photolysis has confirmed the importance of channel 1a but has suggested the existence of other nitrogen-containing channels.

Dynamics of the Photoproducts. In the present investigation we have observed and quantified production of NO_3 in the 248 nm photodecomposition of PAN. The NO_3

product was diagnosed unambiguously through its characteristically strong visible fluorescence. However, a complication to the quantification of the NO_3 yield was presented by fluorescence from highly excited NO_2 photoproduct. Although the occurrence of electronically and vibrationally excited NO_2 in the photolysis of a number of nitrates has been characterized previously,¹ the present study evidenced a dramatic increase in the apparent absorption cross section of NO_2 around 630 nm. We have been able to rationalize this increase in terms of the amount of internal excitation of the NO_2 photoproduct. More importantly, we were able to eliminate the potential fluorescence interference due to excited NO_2 photoproduct by confining the experimental fluorescence measurements to sufficiently high pressures and long delay times following PAN excitation.

NO_3 Quantum Yield Determination. A NO_3 quantum yield of 0.3 ± 0.1 was derived from the experimental measurements. Assuming that $(\phi_{1a} + \phi_2) = 1$, this result is consistent with the previously measured NO_2 quantum yield of 0.83 ± 0.09 , within the combined errors of the measurements. The quantum yield results strongly indicate that NO_2 and NO_3 are the only nitrogen-containing products of PAN photolysis at 248 nm.

Atmospheric Implications. Atmospheric production of PAN is most rapid near continental sites of large NO_x and hydrocarbon emissions. However, due to the high sensitivity of PAN to typical tropospheric temperatures (i.e. PAN thermal lifetime increases by factor of 100 for 250 C decrease in temperature), global tropospheric distributions of PAN are shifted towards higher altitudes and are heavily influenced by transport meteorology.² The combination of these factors enables PAN to serve as an important intermediate in the redistribution of NO_x from its source areas to the remote free troposphere.

Above approximately 7 km, photolysis replaces thermolysis as the primary loss mechanism of PAN. Accordingly, the potential role of PAN in free troposphere NO_x and O_3 chemistry is determined by the rate and mechanistic details of the photolytic process.

In particular, production of NO_3 and $\text{CH}_3\text{C}(\text{O})\text{O}$, as opposed to NO_2 and $\text{CH}_3\text{C}(\text{O})\text{O}_2$, in PAN photolysis results in additional odd oxygen production through rapid photochemical decomposition of NO_3 and $\text{CH}_3\text{C}(\text{O})\text{O}$



where the methyl radical generated in reaction 17 can give rise to as many as three odd oxygen species during its subsequent oxidation to CO_2 . The importance of this potential impact on ozone production can be gauged by comparison to the major sources of O_x which are



For low- NO_x remote free tropospheric conditions (i.e. $[\text{NO}] \approx 20 \text{ pptv}$, $[\text{RO}_2] < [\text{HO}_2] \approx 5 \text{ pptv}$),²¹ reaction 18 is responsible for odd oxygen production rates on the order of 500 pptv d^{-1} . Odd oxygen production rates from PAN photolysis are substantially less than this ($\approx 40 \text{ pptv d}^{-1}$) given typical PAN mid-latitude, clear-sky, photolysis rates ($J_{\text{PAN}} \approx 3 \times 10^{-2} \text{ d}^{-1}$) and largest observed PAN mixing ratios ($> 200 \text{ pptv}$).²² Consequently, extremely polluted, PAN-containing, air masses would have to be advected rapidly in order to significantly affect ozone production in remote locations.

Owing to the presence of a small (i.e. 10%) NO producing channel in NO_3 photolysis,



another potential consequence of NO_3 production in PAN photolysis is a shift, towards increased NO, in the partitioning of atmospheric NO_x in models that previously used only reaction 1a. The NO: NO_2 ratio is mainly determined by the competition between NO_2 photolysis and reactions of NO with HO_2 , RO_2 , and O_3



$$\text{NO/NO}_2 \approx J_{18}/(k_{17}[\text{HO}_2]+k_{18}[\text{RO}_2]+k_{21}[\text{O}_3]) \quad (22)$$

In order for PAN to affect the NO:NO₂ ratio the production rate of NO (via reactions 2 and 16b) from PAN photolysis must approach the rate of NO₂ photolysis. The latter rate is typically on the order of 10000 pptv d⁻¹ ($J(\text{NO}_2) \approx 500 \text{ d}^{-1}$, $[\text{NO}_2] \approx 20 \text{ pptv}$),⁹ which far exceeds the overall PAN photolysis rate given above. From this calculation it is clear that cycling between NO_x species in the upper troposphere is much faster than the cycling of NO_y between active (i.e. NO_x) and reservoir (e.g. PAN) species. Accordingly, although PAN photolysis may impact the overall levels of NO_x in the remote free troposphere, as indicated by Moxim et al.,² the partitioning of nitrogen oxides in PAN photolysis will have little influence on the ambient NO/NO₂ partitioning.

Acknowledgments. The research described in this paper was carried out at the Jet Propulsion Laboratory, California Institute of Technology, under contract with the National Aeronautics and Space Administration. We thank Drs. R. Salawitch and L. Jaegle for their insightful comments on modeling atmospheric PAN, Dr. W. B. DeMore for the use of lasers from his laboratory, Dr. P. S. Stevens for helpful discussions on pumping red dyes with a CVL, and Dr. C. Roehl for comments on the manuscript.

References

- (1) Kleindienst, T.E. *Res. Chem. Intermed.* **1994**,*20*,335, and references within.
- (2) Moxim, W, J.; Levy II, H.; Kasibhatla, P. S. *J.Geophys. Res.* **1996**, 101, 12621, and references within.
- (3) Aikin, A. C.; Herman, J. R.; Maier, E. J, R.; McQuillan, C. *J. Planet. Space Sci.* **1983**, *31*,1075.
- (4) Orlando, J. J.; Tyndall, G. S.; Calvert, J. G.; *Atmos. Environ.* **1992**, *26A*, 3089.
- (5) Roberts, J. M.; Bertman, S. B. *In?. J.Chem.Kinetics* **1992**,*24*,297.
- (6) Grosjean, D; Grosjean, E.; Williams, E. L., II *J. Air & Waste Manage. Assoc.* **1994**,*44*, 391.
- (7) Talukdar, R. K.; Burkholder, J. B.; Schmoltner, A. -M.; Roberts, J. M.; Wilson, R. R.; Ravishankara, A. R. *J. Geophysical Res.* **1995**,*100*, 14163,
- (8) Mazely, T. L.; Friedl, R. R.; Sander, S. P. *J.Phys.Chem.* 1995,*99*,8162.
- (9) DeMore, W. B.; Sander, S. P.; Golden, D. M.; Hampson, R. F.; Kurylo, M. J.; Howard, C. J.; Ravishankara, A. R.; Kolb, C. E.; Molina, M. J. *JPL Publication 94-26*; Jet Propulsion Laboratory: Pasadena, CA, 1992.
- (10) Bridier, I.; Caralp, F.; Loirat, H.; Lesclaux, B. V.; Veyret, B.; Becker, K. H.; Reimer, A.; Zabel, F. *J.Phys. Chem.* **1991**,*95*,3594.
- (11) Mazely, T. L.; Friedl, R. R.; Sander, S. P. *J.Chem.Phys.* **1994**,*100*,8040.
- (12) Gaffney, J. S.; Fajer, R.; Senum, G. I. *Atmos. Environ.* **1984**,*18*,215.
- 13) Johnston, H. S., Davis, H. F., Lee, Y. T., *J.Phys.Chem.* , **1996**, 100,4713 and references within.

- (14) Ravishankara, A. R.; Wine, P. H.; Smith, C. A.; Barbone, P. E.; Torabi, A. J. *Geophys. Res.* 1986,91,5355,
- (15) Swanson, D.; Kan, B.; Johnston, H. S. *J.Phys.Chem.* 1984,88,3115.
- (16) Oh, D.; Sisk, W.; Young, A.; and Johnston, H. S. *J.Chem. Phys.* 1986,85,7146.
- (17) Corcoran, T. C.; Beiting, E. J.; Mitchell, M. O., *J. Mol. Spectroscopy* 1992,1,54,
- (18) Okabe, H *Photochemistry of Small Molecules*; John-Wiley and Sons: New York, 1978.
- (19) Senum, G. I.; Lee, Y. -N.; Gaffney, J. S. *J.Phys.Chem.* 1984,88,1269.
- (20) Libuda, H. G.; Zabel, F. *Ber. Bun-Ges.* 1995,99,1205.
- (21) Davis, D. D.; Crawford, J.; Chen, G.; Chameides, W.; Liu, S.; Bradshaw, J.; Sandholm, S.; Sachse, G.; Gregory, G.; Anderson, B.; Barrick, J.; Bachmeier, A.; Collins, J.; Browell, E.; Blake, D.; Rowland, S.; Kondo, Y.; Singh, H.; Talbot, R.; Heikes, B.; Merrill, J.; Rodriguez, J.; Newell, R. E. *J. Geophys Res.* 1996, 101,2111.
- (22) Jacob, D. J.; Heikes, B. G.; Fan, S.-M.; Logan, J. A.; Mauzerall, D. L.; Bradshaw, J. D.; Singh, H. B.; Gregory, G. L.; Talbot, R. W.; Blake, D. R.; Sachse, G. W. J. *Geophys. Res.*, 1996, 101,24235.

**Quantum Yield for Production of NO₃ from
PAN photolysis at 248 nm**

P, Torr	M	ϕ_{NO_3}	N ₂ O ₅ runs	PAN runs	[PAN] x 10 ¹⁴ cm ⁻³
2	Ar	0.2 ± 0.1	5	6	0.5- 2.0
3	Ar	0.2 ± 0.1	2	3	0.8- 1.3
3	He	0.3 ± 0.1	2	3	1.8-2.5
3	O ₂	0.4 ± 0.1	2	4	1.0-4.5
5	Ar	0.4 ± 0.2	3	3	1.6
5	He	0.3 ± 0.1	3	4	1.3
6	O ₂	0.3 ± 0.1	3	3	2.5- 5.0
7	Ar	0.4 ± 0.2	2	1	3.3
7	He	0.4 ± 0.1	3	3	1.6-3.1
10	O ₂	0.2 ± 0.1	3	2	3.6- 4.2
10	He	0.2 ± 0.1	2	1	2.3

Figure Captions

Figure 1: Total probe signal from the excitation of photoproducts from the 248 nm photolysis of 18.6 mTorr N_2O_5 in 2.1 Torr of Helium. The excitation wavelength was 623 nm and the photon detection window was from 650 nm to 750 nm. The probe excitation source was a dye laser pumped with a 10 kHz copper vapor laser. The exponentially decaying background signal from the 248 nm pump laser was removed from the data. The solid line through the data represents a single exponential fit in which the exponent value is set to match expected diffusion loss rate (i.e. 500 s^{-1}); dashed line represents a least squares bi-exponential fit to the data. The signal strength in this figure was achieved by signal averaging 25,000 excimer pump shots.

Figure 2: Early time loss profiles of the LIF signal from N_2O_5 photolysis. The lower trace (circles) is the same data set shown in figure 1, i.e. 18.6 mTorr N_2O_5 in 2.1 Torr Helium. The squares are data from 5.9 mTorr of N_2O_5 in 0.24 Torr of Helium. The solid lines are exponential least square fits to the data. From the fits, the loss rates of the signal are $1900 \pm 200 \text{ s}^{-1}$ and $1600 \pm 300 \text{ s}^{-1}$ for the data at total pressure of 0.24 and 2.1 Torr, respectively. The lack of a linear dependence on pressure indicates that the observed loss signal cannot be rationalized in terms of pure diffusional loss.

Figure 3: Excitation fluorescence spectrum of NO_3 . The NO_3 was generated by the reaction of HNO_3 with F atoms. The total pressure was 1 Torr and the carrier gas was Helium. The relative flows of the 5% F_2 mixture through the microwave discharge, the HNO_3 , and the carrier were varied in order to maximize the signal at 623 nm. The data are shown by the open circles with the error bars being one standard deviation in precision. The signals were normalized to probe laser power. The solid line is the absorption cross section of NO_3 from Reference 9. The signal strengths of the data set was normalized to

best match the solid curve. Note: experimental data points were determined every 0.5 nm over this wavelength range; however, the tabulated absorption cross sections of NO_3 shown in the plot is per unit nm and the maximum is at 623 nm. This may explain the slight offset between measured and predicted maxima,

Figure 4: Excitation fluorescence spectra of the photoproducts of N_2O_5 photolysis, taken under conditions of different total pressure. In both parts of the Figure, 8.1 mTorr of N_2O_5 was photolyzed at 248 nm, the time delay between the pump and probe laser was 65 μs , and Argon was used as the buffer gas. The total pressures in part A and B of the Figure are 7.0 and 1.0 Torr, respectively. The solid curve in each is the optical absorption cross section for NO_3 . After normalization to laser power, each data set was scaled such that the signal at 623 nm matched the NO_3 absorption cross section. The data at the higher pressure (part A) mapped the absorption cross section well; however, at low pressures the signal shows very little dependence on wavelength.

Figure 5: Loss profile of the fluorescence signal from the photoproducts of N_2O_5 at two different probe wavelengths. In each profile 3.7 mTorr of N_2O_5 was photolyzed at 248 nm in 5 Torr of Helium, The solid circles correspond to data taken when the probe wavelength was near the 623 nm absorption maximum of NO_3 ; the open circles correspond to a local absorption minimum at 635 nm. The solid lines are least square exponential fits to the data. Note: longer time fluorescence data were employed in the fit to accurately determine the other variables in equation 4, but to better illustrate our point only the earlier time data are plotted.

Figure 6: Fluorescence signal from 248 nm photolysis of 9 mTorr of PAN in 3.0 Torr of Argon. The experimental arrangement was the same as for figure 1, except the repetition rate of the C VL was lowered to 5 kHz. In contrast to figure 1, the contribution of

background probe scatter (S_{scatter}) has been removed for this figure. The earliest data shown was taken at a sufficiently long time delay (175 μs) such that the majority of excited photoproducts have relaxed and the subsequent loss rates can be described by a simple exponential, as shown by the curve.

FIGURE 1

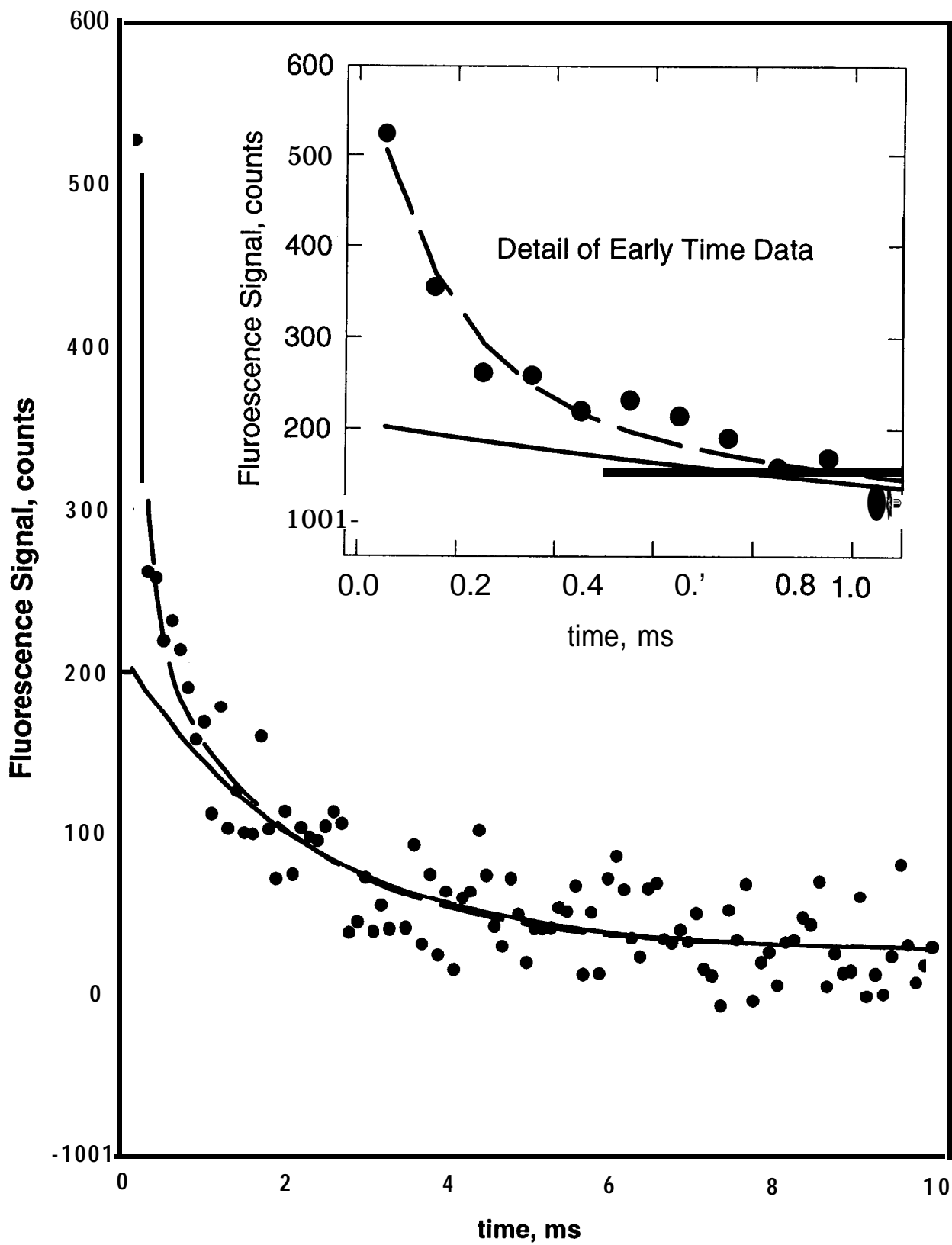


FIGURE 2

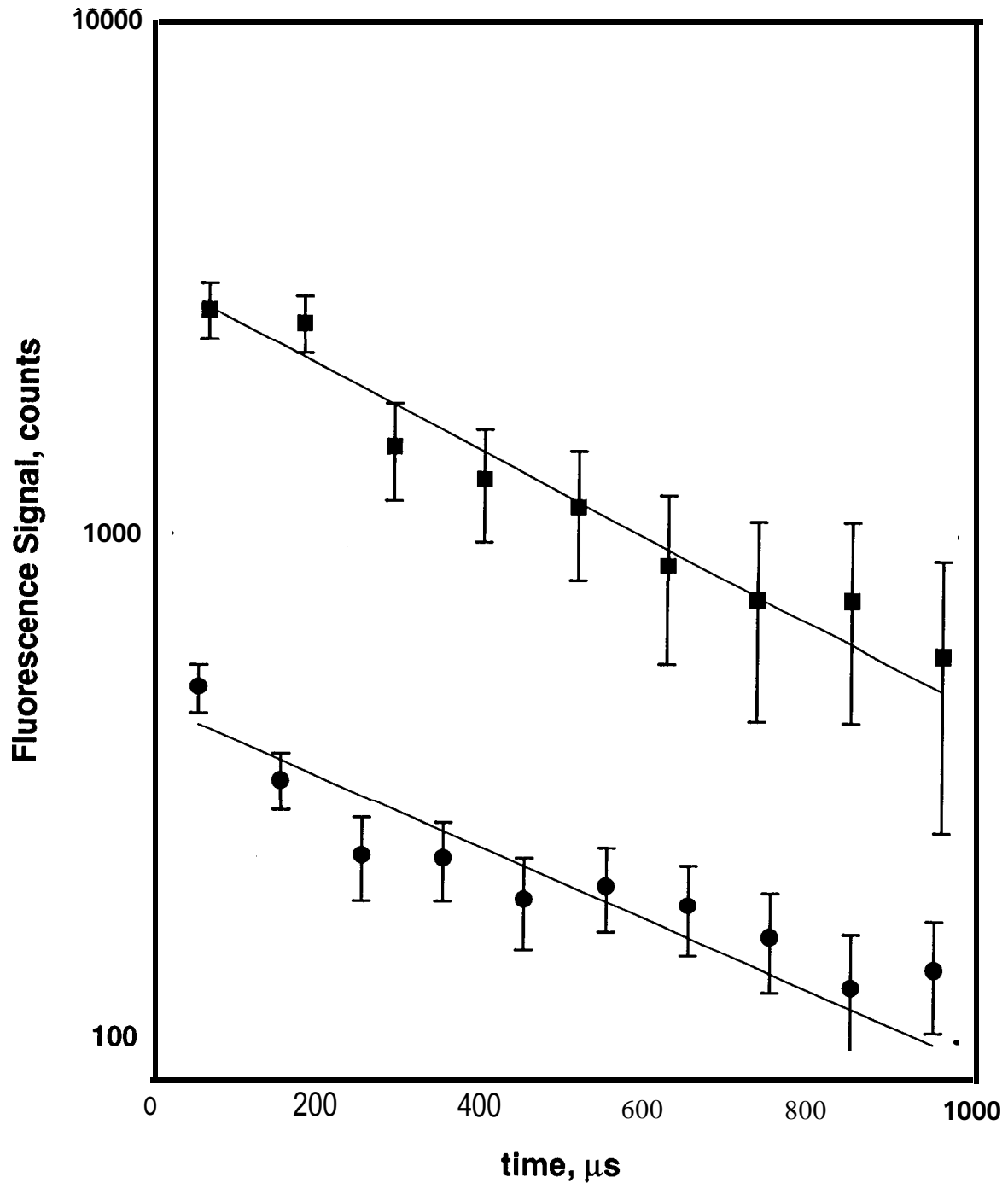


FIGURE 3

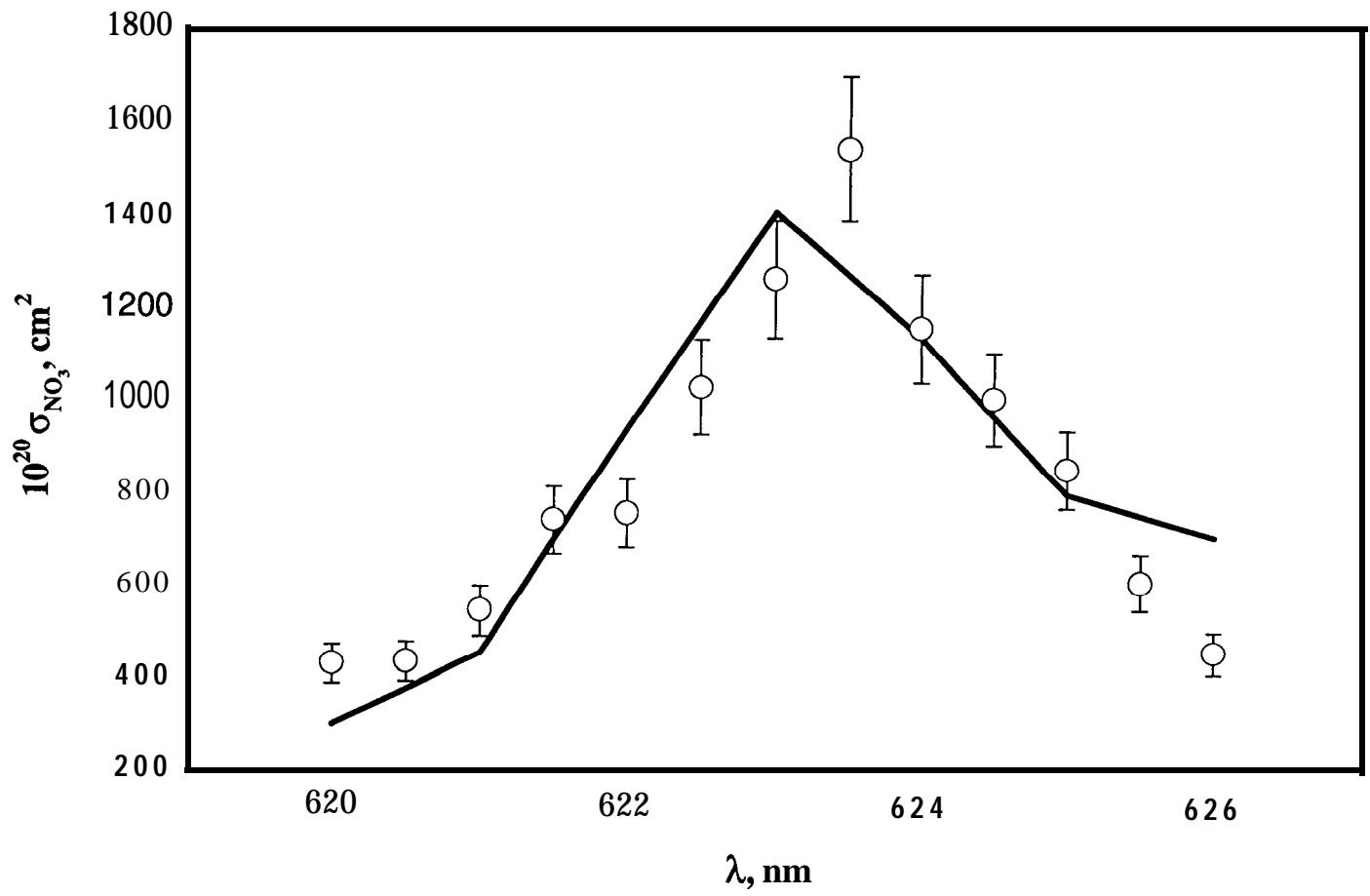


FIGURE 4

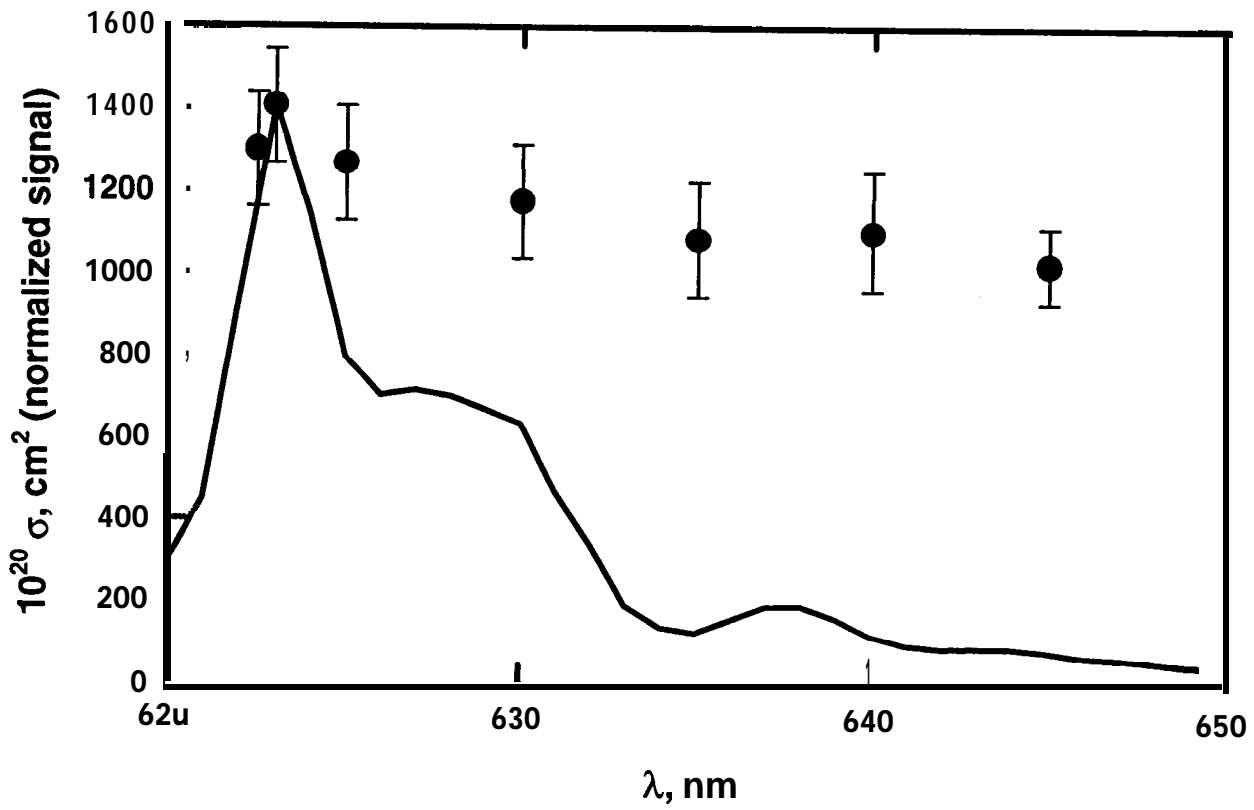
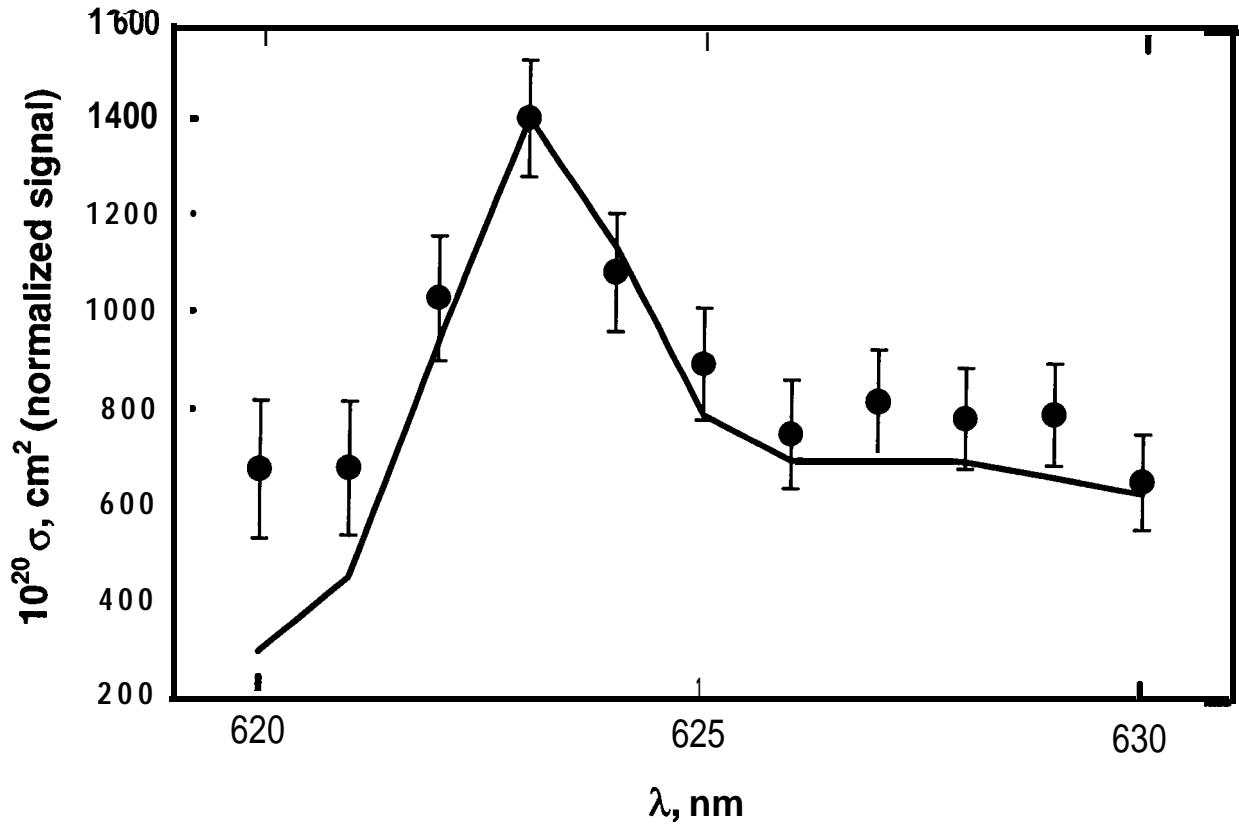


FIGURE 5

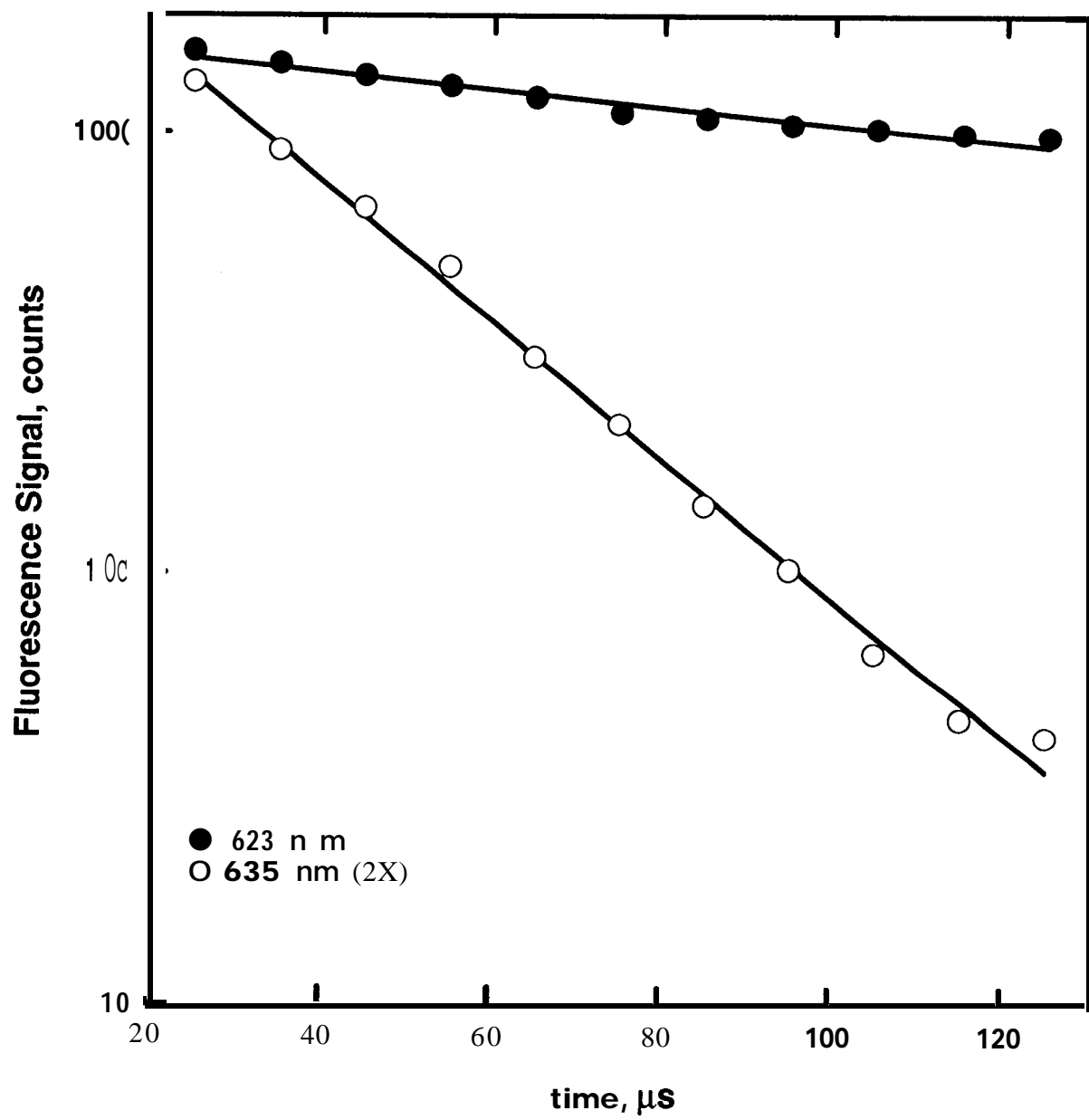


FIGURE 6

